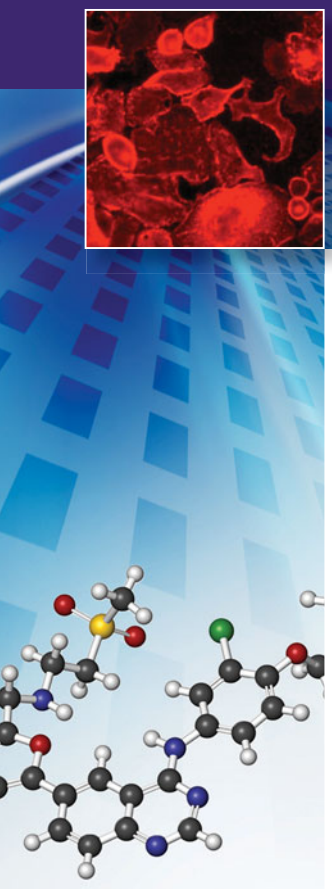


Transmission electron microscopy of specimens and processes in liquids

Frances M. Ross, Chongmin Wang, and Niels de Jonge

The following article is based on the Innovation in Materials Characterization Award presentation given at the 2016 MRS Spring Meeting in Phoenix, Ariz. The authors received this award for their "seminal contributions to the imaging of specimens in liquids using transmission electron microscopy, revolutionizing the direct observation of materials processes, batteries during operation, and biological structures."

Transmission electron microscopy is a powerful technique for the analysis of solid samples, but it can also be used to image in liquid environments, gaining a unique view of processes and structures in liquids. Here, we describe recent developments in electron microscopy of liquids and discuss applications in several areas. We first describe closed-liquid-cell microscopy with its opportunities for visualizing electrochemical processes. We then discuss imaging of low-vapor-pressure liquids relevant to the operation of rechargeable batteries. Finally, we describe imaging of thick biological materials to obtain information on membrane proteins in intact mammalian cells that cannot be observed classically under dry or frozen conditions. Electron microscopy in liquid environments is developing rapidly and has the potential to solve key problems in materials science, physics, chemistry, and biology.

Introduction

Transmission electron microscopy (TEM) is such a powerful technique for obtaining high-resolution spatial and chemical information about solid samples that it has always been tempting to apply it to liquid samples as well. During the past decade, this goal has been realized, and TEM of liquid samples has become a widely used microscopy method.[1,2] Implementing TEM of liquid samples required overcoming two technological challenges. First, most liquids do not exhibit a sufficiently low vapor pressure to remain stable in the vacuum environment of the TEM. Second, it is necessary to control the physical location of the liquid to create a geometry compatible with TEM. Early pioneers of electron microscopy recognized these two issues in the 1940s.[3,4] Their early work set the stage for two experimental strategies, which are referred to as open- and closed-cell (or chamber) approaches; these still form the basis of electron microscopy in liquids (**Figure 1**). In open-cell microscopy,[3,5] the pressure around the sample is controlled using differential pumping to maintain a vacuum in the rest of the system that is good enough to operate the microscope (Figure 1a). In closed-cell microscopy,[4,6] the liquid is enclosed between two closely spaced electron-transparent membranes (Figure 1b). By physically confining the liquid within a thin layer, imaging is possible in transmission mode through the windows and liquid.

Despite this impressive progress, electron microscopy of liquids did not become widely popular because of the engineering challenges involved. Closed cells used relatively thick windows (made, for example, of carbon) and thick liquid layers, so they generally did not provide a resolution that was much better than that of light microscopy. In open-cell TEM, it was difficult to control the liquid/vapor environment, and the analogous open-cell use of environmental scanning electron microscopy (ESEM) for studying liquids remained underappreciated because the lower beam energy (and other factors) prevented high-resolution imaging. Biologists turned to rapid freezing to prepare samples for imaging, while materials scientists found other problems to solve.

The use of electron microscopy for high-resolution and *in situ* investigations of liquids had to await advances in microfabrication to provide solutions to the technical challenges.

Frances M. Ross, IBM T.J. Watson Research Center, USA; fmross@us.ibm.com
Chongmin Wang, Environmental Molecular Sciences Laboratory, Pacific Northwest National Laboratory, USA; chongmin.wang@pnnl.gov
Niels de Jonge, INM-Leibniz Institute for New Materials, Germany; niels.dejonge@leibniz-inm.de
doi:10.1557/mrs.2016.212

© 2016 Materials Research Society

https://doi.org/10.1557/mrs.2016.212 Published online by Cambridge University Press

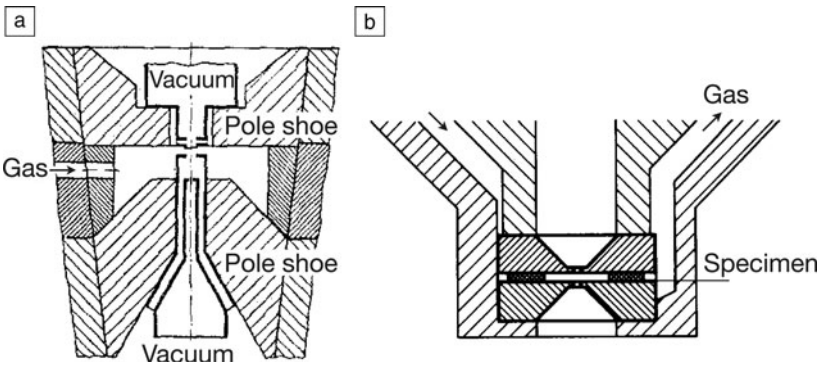


Figure 1. Designs for closed- and open-liquid-cell transmission electron microscopy (TEM). (a) Transmission electron microscope with differentially pumped environmental chamber for imaging specimens at higher pressures. The specimen in a gaseous environment is separated from the high vacuum of the electron column via pump-limiting apertures. The apertures are placed on the pole pieces (labeled "pole shoe") of the objective lens. (b) Environmental chamber enclosed by thin windows. Two aperture holders support thin films and are placed face to face in the upper pole piece of the objective lens. A thin film between the aperture holders serves as a spacer of about 5 μm thickness. (a) Reprinted with permission from Reference 3. © 1942 Springer. (b) Reprinted with permission from Reference 6. © 1960 Springer.

In particular, for closed-cell electron microscopy, silicon nitride films supported on silicon microchips were found to act as robust, transparent windows that could withstand more than an atmosphere of pressure difference and could readily be produced in the required dimensions.[7] Water can be placed[8,9] or flowed[10,11] between two such windows for observation in the microscope. Additional microfabrication steps allow incorporation of electrodes[7,12] in the liquid enclosure, increasing the functionality. Even thinner materials such as graphene can be used as windows,[13,14] although (at present) with a less well-controlled liquid geometry and functionality. For open-cell experiments, low-vapor-pressure liquids such as ionic liquids can be integrated within microfabricated or micromanipulator-based sample holders to enable a variety of *in situ* experiments.[15] Liquid samples have been studied with both TEM and scanning transmission electron microscopy (STEM). TEM can provide higher temporal resolution, while STEM provides excellent contrast for materials of high atomic number in liquids. STEM can be used in dedicated instruments, in combined TEM/STEM instruments, or as the detection mode through thin liquid samples in ESEM.[16]

In this article, we aim to indicate the current state, scope, and opportunities available with TEM and STEM of liquid samples by focusing on three applications. We first discuss the design of closed liquid cells (sometimes called liquid micro-chambers) for TEM, with a particular emphasis on electrochemical processes. We then describe open-cell (or open-chamber) experiments for low-vapor-pressure liquids, showing processes relevant to battery operation. We finally describe how to adapt liquid-phase electron microscopy to study biological materials in their native environment. Biological materials present an additional challenge related to sample thickness; for instance, mammalian cells can be several micrometers thick. We discuss STEM imaging of labeled proteins in thick water layers, as well as STEM detection in ESEM that allows similar imaging in a native environment.

Closed-cell TEM for electrochemical reactions

Electrochemical setup, beam effects, and resolution

Our interest in putting liquids in the TEM came about as a result of the excitement surrounding porous silicon after its optical emission properties were discovered in 1990.[17] A liquid-phase (hydrofluoric acid) anodic etching process creates the porous network. To observe this process *in situ*, we attempted to etch a thin doped Si layer sandwiched between two undoped layers.[18] Problems with this design led to the use of silicon nitride as a more reliable means to enclose a liquid, using a spacer layer to control liquid thickness and a glued vacuum seal.[19] This simpler design enabled a more general type of experiment. In particular, electrochemical processes could be examined by incorporating electrodes within the liquid cell. The early cells, glued by hand and with low success rates, have now been superseded by improved designs with various functionalities now available commercially and from academic laboratories.[11,12,20–22]

Closed-liquid-cell electron microscopy turns out to be well suited for electrochemical explorations, because it fills an important niche in terms of temporal and spatial resolution that is not addressed by other techniques. It occupies the gap between light microscopy,[23] which has good temporal resolution but limited spatial resolution, and scanning tunneling microscopy (**Figure 2**). Scanning probe techniques can have remarkable resolution in liquids,[24] but the frame rate is limited by the physical scan speed, and it is challenging to access rough liquid/solid interfaces.

This leads us to consider the important question of what resolution we should expect from a closed-liquid-cell experiment. In TEM, thicker samples generally reduce the resolution due to multiple scattering and energy loss of the transmitted electrons.[1] Resolution is improved by making both the liquid and the windows as thin as possible. However, too thin of a liquid layer may not support realistic physical phenomena. For electrochemical experiments in particular, where diffusion often dominates the process under study, a compromise must be made where the liquid is thick enough to allow the experiment to represent the "real life" process, yet thin enough to provide reasonable resolution.

A second consideration in liquid-cell electron microscopy—for all experiments, not just electrochemical investigations—is the effect of the electron beam.[25] Sample–beam interactions in TEM have been well studied for solid samples, but for liquids, we can use the literature from medical and reactor physics.

https://doi.org/10.1557/mrs.2016.212 Published online by Cambridge University Press

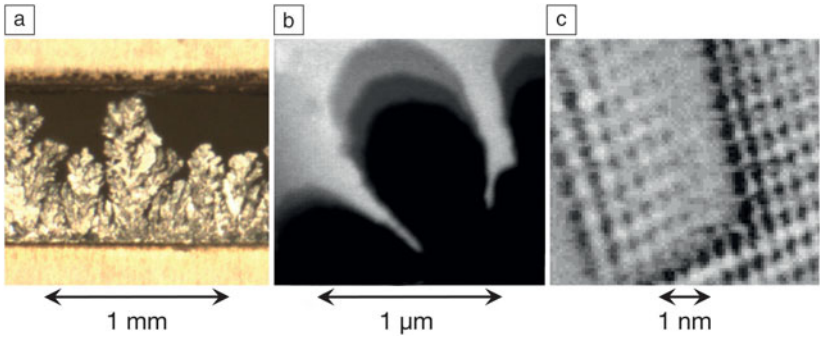


Figure 2. Comparison of imaging techniques for electrochemistry indicating the available resolution. (a) Light microscopy: Deposition of Zn in alkaline electrolyte, from a video at 30 images per s. (b) Liquid-phase transmission electron microscopy: Progression of the growth front during potentiostatic Cu deposition from $H_2SO_4/CuSO_4$. Three images from a video are superimposed showing the advancing growth front.[20] (c) Scanning tunneling microscopy: Dynamic changes in the structure of the Cu(100) surface in 0.01M HCl at a voltage of –0.23 V_{SCE} (where V_{SCE} is the potential with respect to a saturated calomel electrode). One image is shown from a sequence recorded at 10 images per s during "collective" growth of a terrace segment several rows wide. (a) Reprinted with permission from Reference 23. © 2010 The Electrochemical Society. (c) Reprinted with permission from Reference 24. © 2001 Elsevier.

The electron beam deposits energy that breaks bonds to create radiolytic species that then react to generate a cascade of other products. In water, a several hundred keV electron beam can produce strong effects at the high dose rates typical of TEM imaging.[26]

Models for water radiolysis, adapted to apply to TEM,[27,28] show that radiolysis products quickly reach a steady-state concentration that depends on the dose rate, and can be rather different from the initial state of the sample. The pH can be changed by irradiation (generally becoming more acidic), radiolytic hydrogen can form bubbles, and radiolytic hydrated electrons, which are highly reactive electrons surrounded by a shell of water, can react with metal ions in solution to form solid particles within the irradiated area. Because of the sensitivity of electrochemical processes to solution chemistry, beam effects must be modeled, and low-dose imaging and efficient detectors are important.

Examples in electrochemistry

Closed-liquid-cell TEM can address a variety of electrochemical questions, with **Figure 3** illustrating a few of the possibilities. The deposition of copper from an acidified copper sulfate solution is shown in Figure 3a. This process is used in the microelectronics industry to form metallic interconnects, and details of nucleation and grain structure are important in optimizing the results. To image nucleation, we use a liquid cell with electrodes that are electron transparent and also polycrystalline (making them somewhat more relevant to the industrial substrates).[7,19] The single image shown in Figure 3a is taken from a set of movies recorded under constant potential.[29] Nucleation, growth, crystal shape, and coalescence are visible as a function of time.

We simultaneously recorded the current flowing through the liquid cell at each time (see the graph in Figure 3a) and correlated this electrochemical signature with the movie. Such information is helpful in developing models of nucleation and growth, especially as compared to standard analysis where the surface is imaged only *ex situ* after deposition is complete or at fixed times after interrupting growth. The data in Figure 3a were used to identify different pathways by which atoms arrive at the growing nuclei.[29,30]

Once the surface is covered with metal, it is still possible to track deposition by imaging the edge of the electrode as the growth front propagates into the liquid. An example is shown in Figure 3b for the growth of zinc.[31] The growth front has developed an irregular, dendritic appearance. Analysis of the growth front evolution can be carried out over a range of conditions, measuring for example, roughness, local deposition rate, and spatial correlations. This provides the opportunity to examine the physical phenomena that determine growth front stability. Analysis based on fitting classical models for growth front dynamics, such as kinetic roughening and diffusion limited models, can help in understanding what triggers the growth front to become unstable.

Growth front stability is important in battery charge/discharge cycling, where formation of the type of structure shown in Figure 3b could potentially short out the battery.[32] For zinc-based batteries, which otherwise have many environmental and cost benefits, dendrite formation is a particular problem, reducing cycle life.[23] Liquid-cell TEM allows us to evaluate strategies that have been developed to maintain growth-front planarity, such as the use of additives and pulse plating. As an example, the two images in Figure 3b compare similar growth with and without the presence of an inorganic additive, Bi_2O_3. The additive does not suppress instabilities, but delays their onset (Figure 3b, left).[31] It would allow a slightly faster charge rate for a battery—if we first complete the important work of showing that this result also applies to much larger practical systems.

Another electrochemical example where liquid-cell microscopy can be helpful is corrosion. This hugely important problem starts at small features—pinholes, grain boundaries, crevices—making corrosion challenging to analyze using spatially averaged techniques. The images in Figure 3c are from an Al thin film exposed to water in the liquid cell and imaged every few hours.[33] Intragranular pit formation is followed by the formation of voids beneath the passivating oxide layer. The possibilities are exciting, especially if combined with compositional measurements.[34]

Figure 3d shows a related example of the process of galvanic displacement. A solution containing palladium ions is

https://doi.org/10.1557/mrs.2016.212 Published online by Cambridge University Press

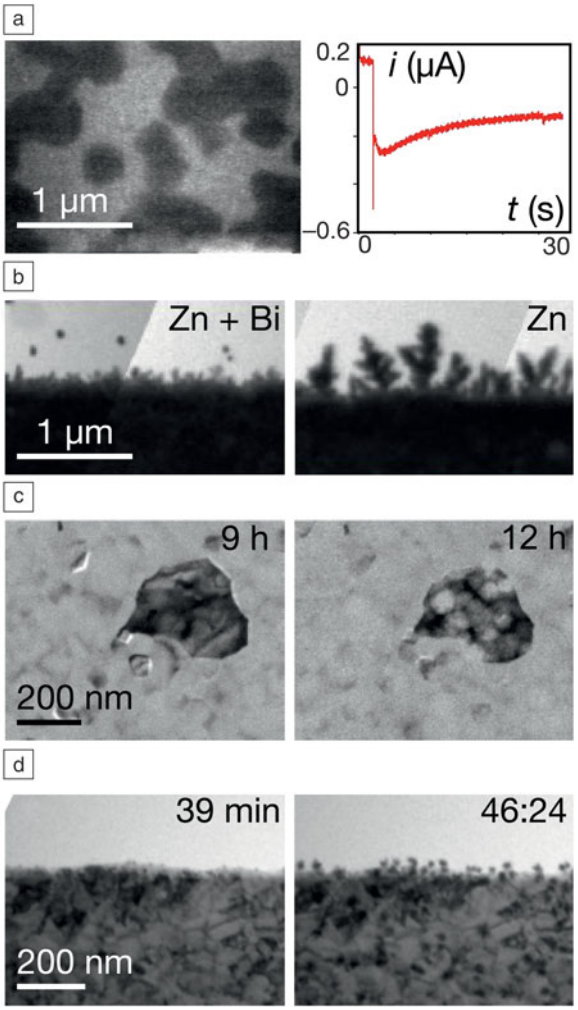


Figure 3. Electrochemical processes imaged using a closed-liquid cell in transmission electron microscopy. (a) Bright-field image from a movie obtained during potentiostatic deposition of Cu islands (dark features) on polycrystalline Au (background), and the complete current (*i*) versus time (*t*) for the movie. The electrolyte is 0.1 M $CuSO_4$ + 0.18 M H_2SO_4, and deposition took place at a constant potential of –70 mV with respect to a Cu reference electrode.[29] (b) Growth instabilities forming during galvanostatic deposition of Zn onto polycrystalline Au. In a pulsed mode, 40 nA was applied (10 s on, 10 s off for 20 cycles). The electrolyte is 0.5 M $ZnSO_4$ + 0.1 M H_2SO_4 for both images, but with the addition of 0.25 mM Bi_2O_3 in the left-hand image. The Bi does not suppress dendrites, but it delays their development by favoring Zn growth between the asperities. (c) Formation of intragranular pits in a coarse-grained Al film after exposure to distilled water in a closed-liquid cell for the times indicated.[33] (d) Galvanic displacement of Ni by Pd. The right-hand image shows Pd nanostructures (dark features) that formed after flow of 0.18 M H_2SO_4 + 0.025 M $PdSO_4$.

flowed over a nickel surface, and Pd is deposited as the "less noble" metal as Ni goes into solution. Liquid-cell TEM provides a good way to access the microstructural details of this type of process.[35] Here, Pd is seen in the second image to deposit in the form of nanoparticles, creating a nanostructured Pd/Ni surface that has useful catalytic properties, for example, for subsequent electroless deposition of magnetic materials.

These examples illustrate some of the electrochemical processes that are accessible with closed-liquid-cell TEM. The key benefit is the combination of electrochemical measurements with structural information obtained with a temporal and spatial resolution that cannot be achieved using other techniques. The challenge in using the results to refine electrochemical models is to relate the liquid-cell data to the larger-scale process. We need to control the experimental geometry, compare with *ex situ* data, and understand and model the sample–beam interactions and liquid flow patterns.

With careful quantification, and continuing improvements in the closed-cell experimental technique, we anticipate exciting opportunities involving heating, cooling, different electrode geometries and materials, and well-controlled liquid flow. Advanced electron microscopy techniques including high-speed image acquisition, analytical microscopy, aberration-corrected microscopy, and correlative microscopy, which we discuss next in the context of biological materials, will extend the reach of these *in situ* investigations even further.

Open-cell electrochemical TEM studies of rechargeable battery processes

The fundamental concept of open-cell TEM

Energy storage systems such as rechargeable batteries include multiple components, and these components are closely integrated to allow concordant ionic and electronic transport during functioning.[32] Cyclic charging and discharging of a battery causes structural and chemical evolution of the cathode, anode, electrolyte, and the interfaces between the liquid electrolyte and electrode. It is this evolution of the battery components that, in most cases, directly contributes to capacity fading and the eventual failure of the battery. Designing and discovering new or improved materials for batteries therefore critically relies on a fundamental understanding and direct correlation between structural and chemical evolution and performance. Electron microscopy and spectroscopy in *ex situ* mode is one of the most powerful tools to probe the relevant characteristics of battery materials, comparing microstructural features before and after cycling to yield insights into the relationship between microstructure and battery failure. However, the dynamic nature of cycling and the continuous evolution of the battery components mean that *ex situ* microscopy cannot answer key questions regarding the timing and mechanism of structural and chemical evolution. Direct observation under dynamic operating conditions is preferable.

The development of open-cell TEM techniques has therefore been a major advance for TEM studies of rechargeable batteries.[15,36] Open cells can be used because electrolytes based on ionic liquids with low-vapor pressure can be loaded directly into the TEM vacuum and imaged without the need for windows. At the same time, to make the battery small

https://doi.org/10.1557/mrs.2016.212 Published online by Cambridge University Press

enough to fit into the TEM, a single nanowire can be used to form the observable electrode. The arrangement of such a nanobattery is schematically illustrated in **Figure 4**a.[37] Here we show SnO_2 for the anode and $LiCoO_2$ for the cathode; the electrolyte is 10% lithium bis(trifluoromethanesulfonyl)imide (LiTFSI) dissolved in a hydrophobic ionic liquid, 1-butyl-1-methylpyrrolidium (P_{14}) TFSI (P_{14}TFSI). This electrolyte wets the nanowire surface to form a conformal coating (Figure 4b), which is equivalent to immersion of the electrode material in the electrolyte. In this sense, the open-cell nanobattery configuration can mimic the processes that occur in a real battery. A variation of the open-cell configuration is achieved by using lithium oxide as a solid electrolyte.[38,39]

Although the open-cell nanobattery works well for direct observation of electrode material evolution, we find some deficiencies if we compare it with real batteries. These include modification of kinetics (Li-ion transport and electrode response to ion motion) and the lack of a solid-electrolyte interphase layer. Closed cells allow use of electrolytes that are closer to real battery operation, mitigating the previously discussed shortcomings, but the presence of the windows lowers the resolution. A combination of open- and closed-cell TEM is the best way to achieve an accurate understanding of the operation of these complex materials systems.

Direct observations of lithiation-induced structural and chemical evolution

The open-cell configuration has provided a wealth of information regarding the behavior of metal ions such as Li, Na, and Ca in electrode materials during charge/discharge cycles,[40] directly revealing structural and morphological evolution in anode materials such as Si, Ge, Al_2O_3, SnO_2, ZnO, Sn, graphene, and carbon nanotubes. The lithiation behavior of Si illustrates the complexity of these reactions, as it features lithiation-induced solid-state amorphization, anisotropic volume expansion, a two-phase reaction process, a self-regulated lithiation rate due to stress generation, a phase transition of amorphous Li_xSi to $Li_{15}Si_4$ at a critical composition x, and a critical size for fracture of the Si particles.[41] The lithiation of a silicon nanowire is schematically illustrated in **Figure 5**.

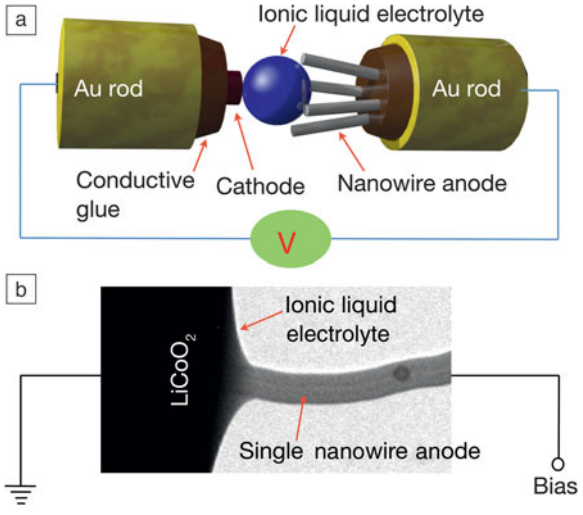


Figure 4. Open-cell transmission electron microscope (TEM) used to examine operation of a nanobattery formed using an ionic liquid as the electrolyte and a 100 nm diameter nanowire as the anode.[37] (a) Schematic drawing showing the experimental configuration. (b) Typical TEM image of the anode of a working nanobattery visualized during cycling.

To illustrate the power of open-cell TEM, consider one stage of this process, the phase transition of amorphous Li_xSi (a-Li_xSi) to crystalline (c-) $Li_{15}Si_4$. A variety of *in situ* and *ex situ* spectroscopy measurements have shown that lithiated a-Li_xSi crystallizes instantaneously to either $Li_{15}Si_4$ or $Li_{22}Si_5$.[42] *In situ* S/TEM provided a detailed atomistic mechanism for this phase transition, revealing that a-Li_xSi transforms to c-$Li_{15}Si_4$ when x reaches a critical value of 3.75, and this phase transition occurs via a congruent process that leads to neither phase segregation nor formation of a residual phase (Figure 5).[41] The congruent phase transformation process does not involve long-range diffusion of the chemical species, only local atomic rearrangement, in contrast to general nucleation and growth processes in which local chemical composition fluctuations lead to phase separation. *In situ* TEM imaging, with its resolution and compositional capability, is a powerful approach for understanding and optimizing the reactions taking place during battery operation.

Liquid-phase STEM for studying membrane proteins in whole mammalian cells

Principles of studying membrane proteins

Liquid-phase electron microscopy has great potential for the study of membrane proteins in mammalian cells.[10,43–47] Membrane proteins (receptors) in the plasma membrane of the cell respond to the presence of small proteins, specifically binding to the receptor (so-called ligands), and then decide what action the cell should take, for example, cell growth. But despite the fact that membrane proteins represent almost one-third of all cellular proteins and two-thirds of current drug targets, many factors governing their function are still unknown.

An example of a membrane protein is the epidermal growth factor receptor (EGFR) (**Figure 6**).[48] This receptor becomes activated upon binding of its ligand (EGF) and then forms a protein complex together with another activated EGFR. This dimerization is followed by a conformational change of the intracellular part of the dimer, which triggers a signal cascade eventually leading to cell growth. To find out exactly what happens at the cell membrane once EGF is present, one would be interested in knowing, for example, in which cellular region or in which cells dimerization takes place, or under which chemical conditions and at which time points. But no one has observed individual proteins in the intact cell. Most of our knowledge about these proteins has

https://doi.org/10.1557/mrs.2016.212 Published online by Cambridge University Press

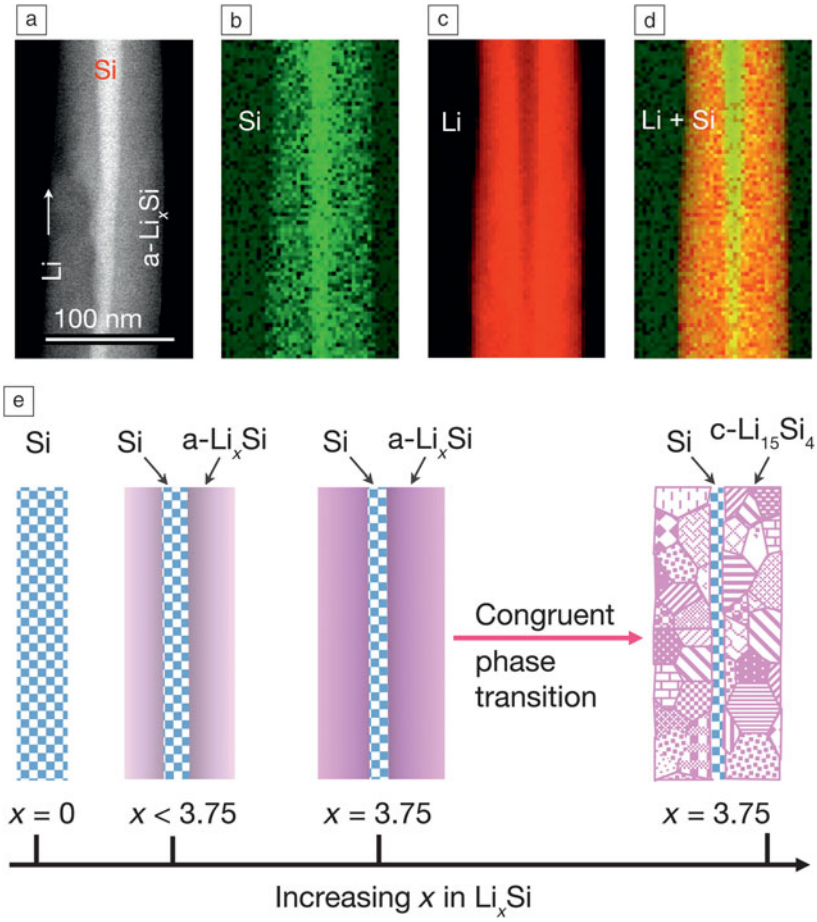


Figure 5. Lithiation process studied with scanning transmission electron microscopy (STEM). (a) STEM annular dark-field image of a Si nanowire anode. Electron energy-loss spectroscopy maps of elemental distribution, (b) Si, (c) Li, and (d) superimposed Li and Si, revealing the core–shell lithiation of the silicon nanowire. (e) Schematic of the silicon nanowire lithiation process and the spontaneous congruent phase transition of amorphous a-Li$_x$Si to crystalline c-Li$_{15}$Si$_4$ when x reaches the critical value of 3.75 in the amorphous phase.[41]

been obtained from indirect biochemical methods where material from thousands of cells is pooled, and cell heterogeneity is thus not taken into account.[46]

To study membrane proteins with liquid-phase STEM, mammalian cells in liquid are enclosed between thin and electron transparent silicon nitride windows separating the sample from the vacuum of the electron microscope (**Figure 7**a). In order to obtain contrast through water and cell material that is several micrometers in thickness, nanoparticles of a material of high density and atomic number (Z) such as gold or fluorescent quantum dots (QDs) are used as specific protein labels. Since the labels may influence the proteins, extensive control experiments are needed. The atomic number contrast in STEM imaging allows these nanoparticles to be detected above the background signal produced by the thick layer of low-Z material.[10,49]

It is not always necessary to enclose the cells fully in liquid in a microfluidic chamber. For many studies, it is sufficient to obtain information from the thin outer regions of the cells, and those can be imaged with high resolution using ESEM with a STEM detector (Figure 7b).[16,50] ESEM works for thinner samples than standard TEM/STEM because of the lower electron-beam energy (30 keV versus 200 keV), but the same principle of Z-contrast applies using the STEM detector in ESEM. Cells in water are kept at 3°C in a sample stage equipped with a Peltier cooling element, and the vacuum level in the specimen chamber is carefully adjusted to around 740 Pa to maintain a thin liquid layer on the sample. Imaging is accomplished with an electron dose below the damage threshold.[51]

For many biological experiments, it is highly desirable to examine not just a randomly selected cellular region, but rather to navigate through many cells and select regions of interest. For this reason, correlative light microscopy and liquid-phase STEM are powerful tools,[52] especially since the microchip with cells presents a simple platform for transferring a sample between the two microscopes.

Research on HER2 in breast cancer cells

As an example of the capabilities of liquid-phase STEM, we describe results obtained for HER2 receptors in breast cancer cells.[46] This receptor of the EGFR family is special because it does not need a ligand to become active; it is an orphan receptor. As a consequence, this protein can trigger cell growth without being controlled by an external signal. This can lead to dysregulation of cell growth in the tumor type that overexpresses HER2.[53] Particularly problematic is that drug resistance develops in many patients,[54] with an origin that is not fully understood.

Figure 8a shows an overview fluorescence image of QD-labeled HER2 in breast cancer cells. These cells differ from each other in morphology and HER2 membrane concentration. The fluorescence and STEM images of a region of interest are shown in Figure 8b–c. The QD labels become visible at higher magnification (Figure 8d). The high spatial resolution of 3 nm allows measurement of the individual positions of all labeled HER2 proteins. The HER2 distances were statistically analyzed and it was found that an interlabel distance of 20 nm occurred more frequently than expected at random. Since the expected center-to-center label distance of two labels attached to a HER2 homodimer amounts to 20 nm, it was deduced that HER2 was present as a homodimer.[46] It was thus possible to quantify the

https://doi.org/10.1557/mrs.2016.212 Published online by Cambridge University Press

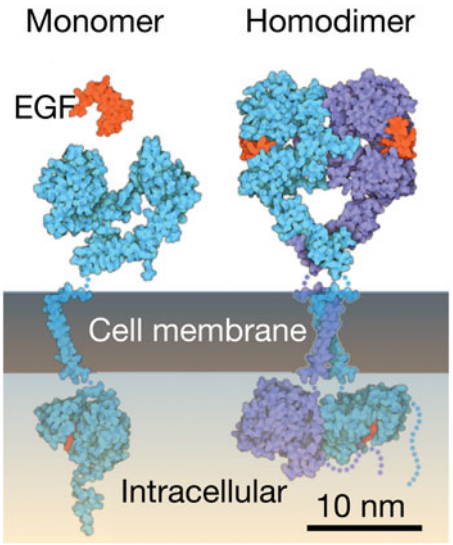


Figure 6. Side view of the HER1 dimer in the plasma membrane. Left: Non-activated HER1 monomer and unbound ligand epidermal growth factor (EGF). Right: Activated HER1 dimer with bound EGF ligand.[48]

stoichiometry of the HER2 complexes, distinguishing between monomers, dimers, and higher-order clusters, and resolving this information per cellular region.

A key finding was the discovery of a small (few percent of the total of cells) sub-population of cells with a different phenotype compared to the average cell.[46] This group of cells was characterized by a flat cytoplasmic border and was identified as resting cells. HER2 homodimers were found to be absent from this subpopulation of cells, even though the membrane concentration of HER2 was similar to that of the majority of cancer cells. We hypothesize that this sub-population of cancer cells plays a critical role in the development of drug resistance because these small sub-populations of cells could possibly respond differently or not at all to the drugs, while they would remain undetected using biochemical methods or conventional microscopy techniques. This example demonstrates both the need for single-cell studies to address cancer cell heterogeneity, and the unique capabilities of liquid phase STEM.

Conclusions

TEM and STEM of liquid samples has developed into a widely used analytical microscopy technique in which nanoscale spatial resolution and video-rate temporal resolution are readily obtained using modern electron microscopes and sample holder systems. The technique has already provided unique scientific information in areas that include electrochemical processes, battery materials evolution and biological materials such as membrane proteins in cells, as well as topics not discussed here such as solution-based materials synthesis and biomineralization. Of particular importance for electrochemistry is the ability to observe materials changes

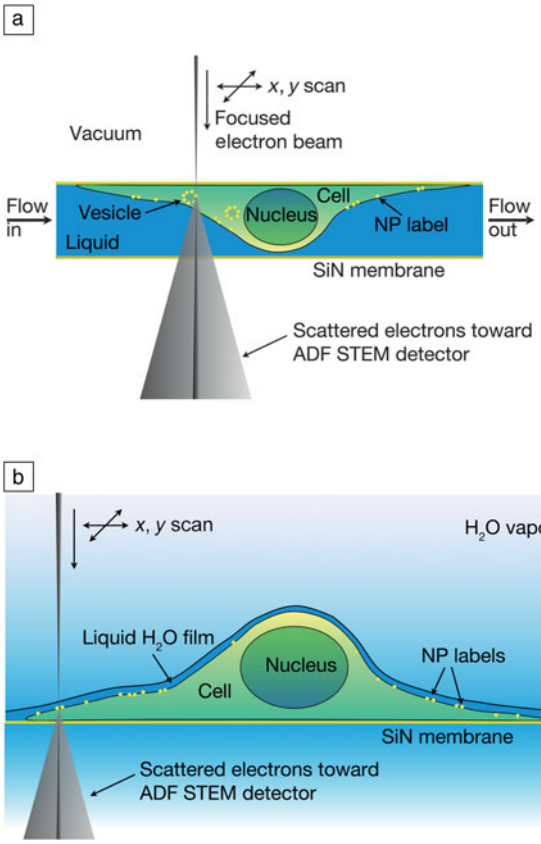


Figure 7. Principles of liquid-phase scanning transmission electron microscopy (STEM) for whole cells. The cell is grown on a supporting silicon nitride (SiN) thin film. Proteins labeled with nanoparticles (NPs) reside in the plasma membrane. As the focused electron beam scans over the cell, the transmitted electrons are recorded using a STEM detector beneath the sample. (a) The cell is fully enclosed in a microfluidic chamber with two windows. (b) The cell is maintained in an atmosphere of saturated water vapor, while a thin layer of cooled water covers the cell, allowing STEM imaging in an environmental scanning electron microscope.[45] Note: ADF, annular dark field.

at the nanoscale while controlling and correlating with electrical potentials and current flow. For biological studies, the key advantage is the few-nanometer resolution for imaging intact cells in a hydrated state.

The solid/liquid interface is centrally important in a wide class of scientific and technological problems. The development of new generations of electrical energy-storage systems relies on a fundamental understanding of mass and charge transport across the solid/liquid interface. Materials synthesis[9] and particle dynamics in liquids,[55,56] surface functionalization, self-assembly, biomineralization[57] and geological phenomena, and liquid-mediated environmental remediation are among the processes that indispensably depend on liquid/solid interfaces and require direct probing of phenomena in liquid. Single-cell studies of biological function[58] and biological macromolecules[59] require imaging through liquid

https://doi.org/10.1557/mrs.2016.212 Published online by Cambridge University Press

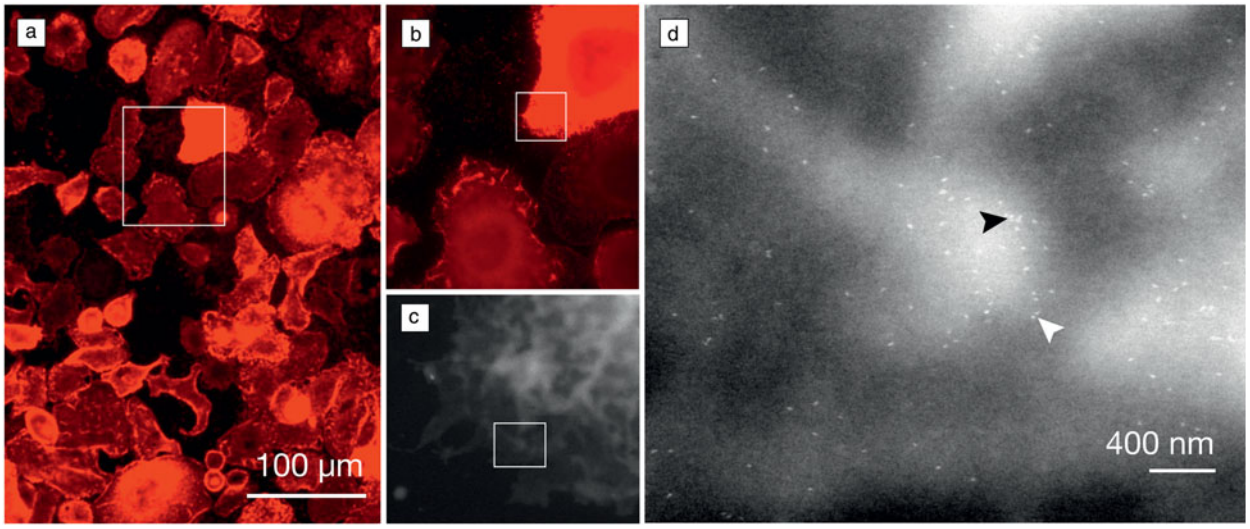


Figure 8. Correlative light and electron microscope overview images of quantum dot-labeled HER2 proteins in SKBR3 human breast cancer cells. (a) Fluorescence overview image showing several dozens of cells. (b) Fluorescence image of the cells within the boxed area in (a). (c) Liquid-phase scanning transmission electron microscope (STEM) image of the boxed region in (b) recorded at 15,000× magnification using environmental scanning electron microscopy. (d) STEM image recorded in the boxed region shown in (c) at 75,000× magnification. The localization of individual HER2 receptors is visible as the bright, bullet-shaped labels. The brighter background represents membrane ruffles. Many pairs (homodimers) are visible; two are indicated with arrowheads.[46]

with good spatial resolution and minimal damage from the probing beam. Accomplishing these and other research tasks places stringent requirements on resolution and dose effects, and requires input from other techniques that provide complementary information. Electron microscopy of liquids is continuously improving in this regard, and has a promising future in addressing a broad variety of interesting problems.

Acknowledgments

F.M.R. acknowledges R.M. Tromp, A.W. Ellis, and M.C. Reuter for their collaborations during the development of the closed liquid cell. N.J. is grateful to D.B. Peckys for biological research and discussions, E. Arzt for his support through INM, and the Leibniz Association. C.M.W. acknowledges the support of the Assistant Secretary for Energy Efficiency and Renewable Energy, Office of Vehicle Technologies of the US Department of Energy (DOE), Contract No. DE-AC02–05CH11231, Subcontract No. 6951379, under the Battery Materials Research Program. Part of the research described here was performed at EMSL, a national scientific user facility sponsored by the DOE's Office of Biological and Environmental Research and located at PNNL.

References

1. N. de Jonge, F.M. Ross, *Nat. Nanotechnol.* **6**, 695 (2011).
2. F.M. Ross, *Science* **350**, aaa9886 (2015).
3. E. Ruska, *Kolloid Z.* **100**, 212 (1942).
4. I.M. Abrams, J.W. McBain, *J. Appl. Phys.* **15**, 607 (1944).
5. G.D. Danilatos, V.N.E. Robinson, *Scanning* **18**, 75 (1979).
6. H.G. Heide, *Naturwissenschaften* **47**, 313 (1960).
7. M.J. Williamson, R.M. Tromp, P.M. Vereecken, R. Hull, F.M. Ross, *Nat. Mater.* **2**, 532 (2003).
8. R. Franks, S. Morefield, J. Wen, D. Liao, J. Alvarado, M. Strano, C. Marsh, *J. Nanosci. Nanotechnol.* **8**, 4404 (2008).
9. H. Zheng, R.K. Smith, Y.W. Jun, C. Kisielowski, U. Dahmen, A.P. Alivisatos, *Science* **324**, 1309 (2009).
10. N. de Jonge, D.B. Peckys, G.J. Kremers, D.W. Piston, *Proc. Natl. Acad. Sci. U.S.A.* **106**, 2159 (2009).
11. E.A. Ring, N. de Jonge, *Microsc. Microanal.* **16**, 622 (2010).
12. R.R. Unocic, R.L. Sacci, G.M. Brown, G.M. Veith, N.J. Dudney, K.L. More, F.S. Walden II, D.S. Gardiner, J. Damiano, D.P. Nackashi, *Microsc. Microanal.* **20**, 452 (2014).
13. J.M. Yuk, J. Park, P. Ercius, K. Kim, D.J. Hellebusch, M.F. Crommie, J.Y. Lee, A. Zettl, A.P. Alivisatos, *Science* **336**, 61 (2012).
14. M. Wojcik, M. Hauser, W. Li, S. Moon, K. Xu, *Nat. Commun.* **6**, 7384 (2015).
15. J.Y. Huang, L. Zhong, C.M. Wang, J.P. Sullivan, W. Xu, L.Q. Zhang, S.X. Mao, N.S. Hudak, X.H. Liu, A. Subramanian, H. Fan, L. Qi, A. Kushima, J. Li, *Science* **330**, 1515 (2010).
16. A. Bogner, G. Thollet, D. Basset, P.H. Jouneau, C. Gauthier, *Ultramicroscopy* **104**, 290 (2005).
17. L.T. Canham, *Appl. Phys. Lett.* **57**, 1046 (1990).
18. F.M. Ross, P.C. Searson, *Proc. 53rd Annu. Microsc. Soc. Amer. Meet.* G.W. Bailey, R.A. Hennigar, N.J. Zaluzec, Eds. (Jones and Begell Publishing, New York, 1995), pp. 232.
19. F.M. Ross, *IBM J. Res. Dev.* **44**, 489 (2000).
20. J.M. Grogan, N.M. Schneider, F.M. Ross, H.H. Bau, *J. Indian Inst. Sci.* **92**, 295 (2012).
21. C. Mueller, M. Harb, J.R. Dwyer, R.J.D. Miller, *J. Phys. Chem. Lett.* **4**, 2339 (2013).
22. J.F. Creemer, S. Helveg, G.H. Hoveling, S. Ullmann, A.M. Molenbroek, P.M. Sarro, H.W. Zandbergen, *J. Microelectromech. Syst.* **19**, 254 (2010).
23. J.W. Gallaway, D. Desai, A. Gaikwad, C. Corredor, S. Banerjee, D. Steingart, *J. Electrochem. Soc.* **157**, A1279 (2010).
24. O.M. Magnussen, L. Zitzler, B. Gleich, M.R. Vogt, R.J. Behm, *Electrochim. Acta* **46**, 3725 (2001).
25. P. Abellan, T.J. Woehl, L.R. Parent, N.D. Browning, J.E. Evans, I. Arslan, *Chem. Commun.* **50**, 4873 (2014).
26. D.B. Peckys, G.M. Veith, D.C. Joy, N. de Jonge, *PLoS One* **4**, e8214 (2009).
27. N.M. Schneider, M.M. Norton, B.J. Mendel, J.M. Grogan, F.M. Ross, H.H. Bau, *J. Phys. Chem. C* **118**, 22373 (2014).

https://doi.org/10.1557/mrs.2016.212 Published online by Cambridge University Press

28. J.M. Grogan, N.M. Schneider, F.M. Ross, H.H. Bau, *Nano Lett.* **14**, 359 (2014).
29. A. Radisic, P.M. Vereecken, J.B. Hannon, P.C. Searson, F.M. Ross, *Nano Lett.* **6**, 238 (2006).
30. A. Radisic, P.M. Vereecken, P.C. Searson, F.M. Ross, *Surf. Sci.* **600**, 1817 (2006).
31. J.H. Park, D.A. Steingart, N.M. Schneider, S. Kodambaka, F.M. Ross, *Nano Lett.* (forthcoming).
32. J.M. Tarascon, M. Armand, *Nature* **414**, 359 (2001).
33. S.W. Chee, F.M. Ross, D. Duquette, R. Hull, "Studies of Corrosion of Al Thin Films Using Liquid Cell Transmission Electron Microscopy," *Mater. Res. Soc. Symp. Proc.* **1525** (Materials Research Society, Warrendale, PA, 2013), p. 558.
34. N.J. Zaluzec, M.G. Burke, S.J. Haigh, M.A. Kulzick, *Microsc. Microanal.* **20**, 323 (2014).
35. E. Sutter, K. Jungjohann, S. Bliznakov, A. Courty, E. Maisonhaute, S. Tenney, P. Sutter, *Nat. Commun.* **5**, 4946 (2014).
36. C.M. Wang, W. Xu, J. Liu, D.W. Choi, B. Arey, L.V. Saraf, J.G. Zhang, Z.G. Yang, S. Thevuthasan, D.R. Baer, N. Salmon, *J. Mater. Res.* **25**, 1541 (2010).
37. C.M. Wang, *J. Mater. Res.* **30**, 326 (2015).
38. X.H. Liu, J.Y. Huang, *Energy Environ. Sci.* **4**, 3844 (2011).
39. F. Wang, H.-C. Yu, M.-H. Chen, L. Wu, N. Pereira, K. Thornton, A. Van der Ven, Y. Zhu, G.G. Amatucci, J. Graetz, *Nat. Commun.* **3**, 1201 (2012).
40. Y. He, M. Gu, H. Xiao, L. Luo, Y. Shao, F. Gao, Y. Du, S.X. Mao, C.M. Wang, *Angew. Chem. Int. Ed.* **55**, 6244 (2016).
41. M. Gu, Z.G. Wang, J.G. Connell, D.E. Perea, L.J. Lauhon, F. Gao, C.M. Wang, *ACS Nano* **7**, 6303 (2013).
42. T.D. Hatchard, J.R. Dahn, *J. Electrochem. Soc.* **151**, A838 (2004).
43. T. Kinoshita, Y. Mori, K. Hirano, S. Sugimoto, K. Okuda, S. Matsumoto, T. Namiki, T. Ebihara, M. Kawata, H. Nishiyama, M. Sato, M. Suga, K. Higashiyama, K. Sonomoto, Y. Mizunoe, S. Nishihara, C. Sato, *Microsc. Microanal.* **20**, 469 (2014).
44. N. Liv, D.S. van Oosten Slingeland, J.P. Baudoin, P. Kruit, D.W. Piston, J.P. Hoogenboom, *ACS Nano* **10**, 265 (2016).
45. D.B. Peckys, N. de Jonge, *Microsc. Microanal.* **20**, 346 (2014).
46. D.B. Peckys, U. Korf, N. de Jonge, *Sci. Adv.* **1**, e1500165 (2015).
47. H. Nishiyama, M. Suga, T. Ogura, Y. Maruyama, M. Koizumi, K. Mio, S. Kitamura, C. Sato, *J. Struct. Biol.* **169**, 438 (2010).
48. Epidermal Growth Factor, Protein Data Bank, National Science Foundation, http://dx.doi.org/10.2210/rcsb_pdb/mom_2010_6.
49. N. de Jonge, N. Poirier-Demers, H. Demers, D.B. Peckys, D. Drouin, *Ultramicroscopy* **110**, 1114 (2010).
50. D.B. Peckys, J.P. Baudoin, M. Eder, U. Werner, N. de Jonge, *Sci. Rep.* **3**, 2626 (2013).
51. J. Hermannsdörfer, V. Tinnemann, D.B. Peckys, N. de Jonge, *Microsc. Microanal.* **20**, 656 (2016).
52. M.J. Dukes, D.B. Peckys, N. de Jonge, *ACS Nano* **4**, 4110 (2010).
53. P.J. Brennan, T. Kumagai, A. Berezov, R. Murali, M.I. Greene, *Oncogene* **21**, 328 (2002).
54. T. Vu, F.X. Claret, *Front. Oncol.* **2**, 62 (2012).
55. E.R. White, S.B. Singer, V. Augustyn, W.A. Hubbard, M. Mecklenburg, B. Dunn, B.C. Regan, *ACS Nano* **6**, 6308 (2012).
56. D. Alloyeau, W. Dachraoui, Y. Javed, H. Belkahla, G. Wang, H. Lecoq, S. Ammar, O. Ersen, A. Wisnet, F. Gazeau, C. Ricolleau, *Nano Lett.* **15**, 2574 (2015).
57. P.J. Smeets, K.R. Cho, R.G. Kempen, N.A. Sommerdijk, J.J. De Yoreo, *Nat. Mater.* **14**, 394 (2015).
58. T.J. Woehl, S. Kashyap, E. Firlar, T. Perez-Gonzalez, D. Faivre, D. Trubitsyn, D.A. Bazylinski, T. Prozorov, *Sci. Rep.* **4**, 6854 (2014).
59. M.J. Dukes, R. Thomas, J. Damiano, K.L. Klein, S. Balasubramaniam, S. Kayandan, J.S. Riffle, R.M. Davis, S.M. McDonald, D.F. Kelly, *Microsc. Microanal.* **20**, 338 (2014). □



Frances M. Ross is currently at the IBM T.J. Watson Research Center. She received her BA degree in physics and PhD degree in materials science from the University of Cambridge. Following a postdoc at AT&T Bell Laboratories, she joined the National Center for Electron Microscopy, Lawrence Berkeley National Laboratory and then IBM, building a program around a microscope with deposition and focused ion beam capabilities. Her interests include liquid-cell electron microscopy, epitaxy, nanowires, and electrodeposition. She received the UK Institute of Physics Boys Medal, the MRS Outstanding Young Investigator Award, and the MSA Burton Medal; holds an honorary doctorate from Lund, and is a Fellow of MRS, APS, AAAS, MSA, and AVS. Ross can be reached by email at fmross@us.ibm.com.



Chongmin Wang is a staff scientist at Pacific Northwest National Laboratory. He received his BSc and MSc degrees in physics from Lanzhou University in China and a PhD degree in materials science and engineering from the University of Leeds, UK. He worked at the Max-Planck Institute for Metals Research in Stuttgart, Germany, as an Alexander von Humboldt Research Fellow, the National Institute for Materials Science in Japan, and Lehigh University, where he focused on atomic-level study of grain-boundary structure and chemistry using S/TEM. His research interests include S/TEM and spectroscopy and applications to materials characterization, especially *in situ* and *operando* S/TEM techniques for energy materials applications. He was the recipient of the Microscopy Today Innovation Award, an R&D 100 Award, the Rowland Snow Award from The American Ceramic Society, the Outstanding Invention Award from the Japanese Science and Education Committee, and a PNNL Exceptional Contribution Award. Wang can be reached by email at chongmin.wang@pnnl.gov.



Niels de Jonge is a senior group leader at the INM-Leibniz Institute for New Materials, Germany, and honorary professor of experimental physics, Saarland University, Germany. He received his MSc degree in physics from the University of Amsterdam, The Netherlands, and a PhD degree in natural sciences, specializing in biophysics, from the University of Freiburg, Germany. He worked as a senior scientist at Philips Research, The Netherlands. At Oak Ridge National Laboratory (ORNL), he pioneered STEM of liquid specimens. He then joined Vanderbilt University School of Medicine as an assistant professor of biophysics. His research interests include *in situ* electron microscopy of biological samples and nanoparticles in the liquid phase, and 3D STEM. De Jonge received the ORNL Innovation Award, the ORNL Esprit de Corps Award, and the Microscopy and Microanalysis Best Paper Award. De Jonge can be reached by email at niels.dejonge@leibniz-inm.de.

MRS®
Career Central
The MRS Job Board—
a one-stop shop for all
your recruiting needs!
SERVICES FOR EMPLOYERS
• Quickly and easily post job openings
• Gain added exposure to candidates by purchasing ad space on most-visited web pages
• Browse job seeker resumes and pay only when applicants respond
• Reach targeted and qualified candidates
• Enjoy MRS Member discounts
www.mrs.org/career-central

https://doi.org/10.1557/mrs.2016.212 Published online by Cambridge University Press

MRS Communications



2016
Volume 6, Issue 3

FUNCTIONAL OXIDES PROSPECTIVE ARTICLES

Geometrical lattice engineering of complex oxide heterostructures: a designer approach to emergent quantum states

Xiaoran Liu, **S. Middey**, **Yanwei Cao**, and **M. Kareev**, University of Arkansas, USA; and **J. Chakhalian**, Rutgers University, USA

Epitaxial heterostructures composed of complex oxides have fascinated researchers for over a decade as they offer multiple degrees of freedom to unveil emergent many-body phenomena often unattainable in bulk. Recently, apart from stabilizing such artificial structures along the conventional [001]-direction, tuning the growth direction along unconventional crystallographic axes has been highlighted as a promising route to realize novel quantum many-body phases. Here we illustrate this rapidly developing field of geometrical lattice engineering with the emphasis on a few prototypical examples of the recent experimental efforts to design complex oxide heterostructures along the (111) orientation for quantum phase discovery and potential applications. DOI:10.1557/mrc.2016.24

Frontiers in strain-engineered multifunctional ferroic materials

Joshua C. Agar, **Shishir Pandya**, **Ruijuan Xu**, **Ajay K. Yadav**, **Zhiqi Liu**, **Thomas Angsten**, and **Sahar Saremi**, University of California, Berkeley, USA; **Mark Asta**, University of California, Berkeley, and Lawrence Berkeley National Laboratory, USA; **R. Ramesh**, University of California, Berkeley, USA; and **Lane W. Martin**, University of California, Berkeley, and Lawrence Berkeley National Laboratory, USA

Multifunctional, complex oxides capable of exhibiting highly-coupled electrical, mechanical, thermal, and magnetic susceptibilities have been pursued to address a range of salient technological challenges. Today, efforts are focused on addressing the pressing needs of a range of applications and identifying, understanding, and controlling materials with the potential for enhanced or novel responses. In this prospective, we highlight important developments in theoretical and computational techniques, materials synthesis, and characterization techniques. We explore how these new approaches could revolutionize our ability to discover, probe, and engineer these materials and provide a context for new arenas where these materials might make an impact. DOI:10.1557/mrc.2016.29

Mesocrystal-embedded functional oxide systems

Jan-Chi Yang, National Cheng Kung University, Taiwan; **Heng-Jui Liu**, National Chung Hsing University, Taiwan; and **Ying-Hao Chu**, National Chiao Tung University and Academia Sinica, Taiwan

Mesocrystal—a new class of crystals compared with conventional single crystals and randomly distributed nanocrystal systems—has captured significant attention in recent decades. Current studies have been focused on the advanced synthesis as well as the intriguing properties of mesocrystal. In order to create new opportunities upon functional mesocrystals, they can be regarded as a new functional entirety when integrated with unique matrix environments. The elegant combination of mesocrystals and matrices has enabled researchers to realize enthralling tunabilities and to derive new functionalities that cannot be found in individual components. Therefore, mesocrystal-embedded system forms a new playground towards multifunctionalities. This review article delivers a general roadmap that portrays the enhancement of intrinsic properties and new functionalities driven by novel mesocrystal-embedded oxide systems. An in-depth understanding and breakthroughs achieved in mesocrystal-embedded oxide systems are highlighted. This article concludes with a brief discussion on potential directions and perspectives along this research field. DOI:10.1557/mrc.2016.25

A perspective on perovskite oxide semiconductor catalysts for gas phase photoreduction of carbon dioxide

Chunxiang Huang, **Zhaosheng Li**, and **Zhigang Zou**, Nanjing University, China

Photocatalytic reduction of carbon dioxide (CO_2) into renewable hydrocarbon fuels using solar energy has gained much attention in the effort to conserve energy and enhance carbon cycling. This paper begins with a brief description of the basic concepts of the photocatalytic reduction of CO_2, introduces some experimental challenges in the gas photoreaction system and provides a review of perovskite oxide semiconductor catalysts, including tantalates, niobates, titanates, zirconates and cerates, for use in the gas phase photoreduction of CO_2. The prospects for the future research of CO_2 photoreduction are also presented. DOI:10.1557/mrc.2016.32

https://doi.org/10.1557/mrs.2016.212 Published online by Cambridge University Press

Coupling and competition between ferroelectricity, magnetism, strain, and oxygen vacancies in $AMnO_3$ perovskites

Astrid Marthinsen, Norwegian University of Science and Technology, Norway; **Carina Faber**, ETH Zürich, Switzerland; **Ulrich Aschauer**, ETH Zürich and University of Bern, Switzerland; **Nicola A. Spaldin**, ETH Zürich, Switzerland; and **Sverre M. Selbach**, Norwegian University of Science and Technology, Norway

We use first-principles calculations based on density functional theory to investigate the interplay between oxygen vacancies, *A*-site cation size/tolerance factor, epitaxial strain, ferroelectricity, and magnetism in the perovskite manganite series, $AMnO_3$ (A = Ca^{2+}, Sr^{2+}, Ba^{2+}). We find that, as expected, increasing the volume through either chemical pressure or tensile strain generally lowers the formation energy of neutral oxygen vacancies consistent with their established tendency to expand the lattice. Increased volume also favors polar distortions, both because competing rotations of the oxygen octahedra are suppressed and because Coulomb repulsion associated with cation off-centering is reduced. Interestingly, the presence of ferroelectric polarization favors ferromagnetic (FM) over antiferromagnetic (AFM) ordering due to suppressed AFM superexchange as the polar distortion bends the Mn–O–Mn bond angles away from the optimal 180°. Intriguingly, we find that polar distortions compete with the formation of oxygen vacancies, which have a higher formation energy in the polar phases; conversely the presence of oxygen vacancies suppresses the onset of polarization. In contrast, oxygen vacancy formation energies are lower for FM than AFM orderings of the same structure type. Our findings suggest a rich and complex phase diagram, in which defect chemistry, polarization, structure, and magnetism can be modified using chemical potential, stress or pressure, and electric or magnetic fields. DOI:10.1557/mrc.2016.30

Modifying oxide nanomaterials' properties by hydrogenation

Xiaodong Yan, University of Missouri—Kansas City, USA; **Lihong Tian**, University of Missouri—Kansas City, USA, and Hubei University, China; **Xinyu Tan**, China Three Gorges University, China; **Minjie Zhou**, Hunan Institute of Science and Technology, China; **Lei Liu**, Chinese Academy of Sciences, China; and **Xiaobo Chen**, University of Missouri—Kansas City, USA

Nanomaterials have been intensively studied over the past decades with many advantages over traditional bulk materials in many applications. Nanomaterials' properties are largely governed by their chemical compositions, sizes, shapes, dimensions, morphologies and structures, which are primarily controlled with the chemical and/or physical fabrication methods and processes. This prospective will highlight recent progress on the modifications of oxide nanomaterials' properties by hydrogenation, namely heat treatment under hydrogen or hydrogen plasma environment, for various applications. DOI:10.1557/mrc.2016.33

FUNCTIONAL OXIDES RESEARCH LETTERS

Monolithic Integration of Perovskites on Ge(001) by Atomic Layer Deposition: A Case Study with $SrHf_xTi_{1-x}O_3$

Shen Hu, **Martin D. McDaniel**, **S. Tarelkin**, **Agham Posadas**, and **Chengqing Hu**, The University of Texas at Austin, USA; **HsinWei Wu**, Arizona State University, USA; **Edward T. Yu**, The University of Texas at Austin, USA; **David J. Smith**, Arizona State University, USA; and **Alexander A. Demkov** and **John G. Ekerdt**, The University of Texas at Austin, USA

This work reports the growth of crystalline $SrHf_xTi_{1-x}O_3$ (SHTO) films on Ge(001) substrates by atomic layer deposition. Samples were prepared with different Hf content *x* to explore if strain, from tensile (*x* = 0) to compressive (*x* = 1), affected film crystallization temperature and how composition affected properties. Amorphous films grew at 225 °C and crystallized into epitaxial layers at annealing temperatures that varied monotonically with composition from ~530 °C (*x* = 0) to ~660 °C (*x* = 1). Transmission electron microscopy revealed abrupt interfaces. Electrical measurements revealed 0.1 A/cm^2 leakage current at 1 MV/cm for *x* = 0.55. DOI:10.1557/mrc.2016.36

Density functional theory investigation of the electronic structure and defect chemistry of $Sr_{1-x}K_xFeO_3$

Andrew M. Ritzmann, **Johannes M. Dieterich**, and **Emily A. Carter**, Princeton University, USA

Solid oxide fuel cells (SOFCs) efficiently generate electricity, but high operating temperatures (Top > 800 °C) limit their utility. Reducing Top requires mixed ion–electron conducting (MIEC) cathode materials. Density functional theory is used here to investigate the role of potassium substitutions in the MIEC material $Sr_{1-x}K_xFeO_3$ (SKFO). We predict that such substitutions are endothermic. $SrFeO_3$ and SKFO have nearly identical metallic electronic structures. Oxygen vacancy formation energies decrease by ~0.2 eV when *x*K increases from 0 to 0.0625. SKFO is a promising SOFC MIEC cathode material; however, further experimental investigations must assess its long-term stability at the desired operating temperatures. DOI:10.1557/mrc.2016.23

Non-linearity variation of single junctions and its analysis using nano-prober within fine-grained ZnO-based multilayer varistors

Eiichi Koga and **Yoshiko Higashi**, Panasonic Co., Japan

Direct electrical measurement of single grain boundaries is performed for ZnO-based multilayer ceramic varistors with fine grains of 2 μm, using a nano-prober. The effect of ZnO grains on non-linearity is shown to be significant. The microstructure is comprised at least two non-linear types as good and bad junctions. The numerical ratio of good to bad is estimated to be about one (non-linearity exponent $\alpha max \geq 10$) to two (<10), which is independent of microstructural development as grain growth. The grain control of twinning as well as crystal orientation and donor concentration is considered effective in the further improvement. DOI:10.1557/mrc.2016.19

https://doi.org/10.1557/mrs.2016.212 Published online by Cambridge University Press

Enhancement of oxygen surface exchange on epitaxial $La_{0.6}Sr_{0.4}Co_{0.2}Fe_{0.8}O_{3-\delta}$ thin films using advanced heterostructured oxide interface engineering

Dongkyu Lee, Massachusetts Institute of Technology and Oak Ridge National Laboratory, USA; **Yueh-Lin Lee** and **Xiao Renshaw Wang**, Massachusetts Institute of Technology, USA; **Dane Morgan**, University of Wisconsin–Madison, USA; and **Yang Shao-Horn**, Massachusetts Institute of Technology and Oak Ridge National Laboratory, USA

Engineering of a novel heterostructured oxide interface was used to enhance the oxygen surface exchange kinetics of $La_{0.6}Sr_{0.4}Co_{0.2}Fe_{0.8}O_{3-\delta}$ (LSCF113) thin films. A single-layer decoration of mixed $(LaSr)_2CoO_{4\pm\delta}$ (LSC214) and $La_{1-x}Sr_xCoO_{3-\delta}$ (LSC113) and a double-layer decoration of stacked LSC214 and LSC113 grown on the LSCF113 markedly enhanced the surface exchange coefficients of the LSCF113 by up to ~1.5 orders of magnitude relative to the undecorated LSCF113. It is hypothesized that two different types of surface decorations can enable Sr segregation at the interface and surfaces of LSC113 and LSC214, leading to enhancement of the oxygen surface exchange kinetics of decorated LSCF113. DOI:10.1557/mrc.2016.28

Titanium dioxide nanowires modified tin oxide hollow spheres for dye-sensitized solar cells

Yajie Wang, **Chengbin Fei**, **Rong Zhang**, and **Lixue Guo**, Chinese Academy of Sciences, China; **Ting Shen** and **Jianjun Tian**, University of Science and Technology, China; and **Guozhong Cao**, Chinese Academy of Sciences, China and University of Washington, USA

Tin oxide (SnO_2) hollow spheres modified with titanium dioxide (TiO_2) nanowires (NWs) synthesized by sequential hydrothermal reactions were investigated as photoanodes for dye-sensitized solar cells. Not only does the hydrothermal treatment form numerous short TiO_2 NWs on the surface of SnO_2 spheres, but also passivates the surface of SnO_2. Consequently, the specific surface area of the photoanode and dye loading are almost doubled, at the same time the surface defects and charge recombination are both appreciably reduced. As a result, the short-circuit photocurrent density and open-circuit photovoltage both greatly increased. The power conversion efficiency of the solar cells increases from 0.4% to 2.9%. DOI:10.1557/mrc.2016.34

Elucidating the synergistic mechanism of nickel–molybdenum electrocatalysts for the hydrogen evolution reaction

Ian S. McKay, **Jay A. Schwalbe**, **Emmett D. Goodman**, **Joshua J. Willis**, **Arun Majumdar**, and **Matteo Cargnello**, Stanford University, USA

Nickel–molybdenum (Ni–Mo) materials are widely used functional oxide catalysts for the hydrogen evolution reaction. In this work, we investigate the high activity of Ni–Mo by depositing size-controlled Ni nanocrystals (NCs) onto Mo substrates. We observe a synergistic increase in catalytic activity that does not scale with the Ni–Mo interface length. This evidence points to a bulk electronic interaction of the two metals that is separate from the mechanism of enhancement seen in conventionally co-deposited Ni–Mo electrocatalysts. In addition to elucidating the catalytic behavior of the Ni–Mo system, this work offers a general NC-based paradigm for investigating fundamental interactions and synergistic effects in electrocatalytic materials. DOI:10.1557/mrc.2016.27

Ferromagnetic oxide heterostructures on silicon

Srinivasa Rao Singamaneni, Army Research Office, North Carolina State University, and The University of Texas at El Paso, USA; **J.T. Prater**, Army Research Office and North Carolina State University, USA; **Fan Wu**, North Carolina State University and Princeton University, USA; and **J. Narayan**, North Carolina State University, USA

Heterostructures consisting of two ferromagnetic oxides $La_{0.7}Ca_{0.3}MnO_3$ (LCMO) and $SrRuO_3$ (SRO) were epitaxially grown by pulsed laser deposition onto a silicon (Si) substrate buffered by $SrTiO_3$ (STO)/MgO/TiN. The x-ray scans and electron-diffraction patterns reveal the epitaxial nature of all five layers. From transmission electron microscopy, the thicknesses of the LCMO and SRO layers were estimated to be ~100 and ~200 nm, respectively. The magnetic properties of individual SRO and LCMO layers are in good agreement with the previous studies reported for those individual layers deposited on lattice-matched substrates, such as STO. The LCMO/SRO heterostructures showed enhanced switching field (from 6008 to 7600 Oe), which may originate from the bulk part of the heterostructure. The ability to grow these multifunctional structures on Si provides a route for wafer scale integration with Si, in contrast to oxide substrates that are not suitable for CMOS integration for microelectronics and spintronics applications. DOI:10.1557/mrc.2016.22

PLASMONICS, PHOTONICS, AND METAMATERIALS PROSPECTIVE ARTICLE

Ultraviolet optoelectronic devices based on AlGaN alloys grown by molecular beam epitaxy

Theodore D. Moustakas, Boston University, USA

This paper reviews progress in ultraviolet (UV) optoelectronic devices based on AlGaN films and their quantum wells (QWs), grown by plasma-assisted molecular beam epitaxy. A growth mode, leading to band-structure potential fluctuations and resulting in AlGaN multiple QWs with internal quantum efficiency as high as 68%, is discussed. Atomic ordering in these alloys, which is different from that observed in traditional III–V alloys, and its effect on device performance is also addressed. Finally, progress in UV-light-emitting diodes, UV lasers, UV detectors, electroabsorption modulators, and distributed Bragg reflectors is presented. DOI:10.1557/mrc.2016.26

https://doi.org/10.1557/mrs.2016.212 Published online by Cambridge University Press

PROSPECTIVE ARTICLE

Phase field modeling of intercalation kinetics: a finite interface dissipation approach

Nega A. Zerihun, Addis Ababa Institute of Technology, Ethiopia; and **Ingo Steinbach**, Ruhr-Universität Bochum, Germany

When two materials interact, the processes between the phases determine the functional properties of the compound. Pivotal interface phenomena are diffusion and redistribution of atoms (molecules). This is especially of interest in Lithium ion batteries where the interfacial kinetics determines the battery performance and impact cycling stability. A new phase field model, which links the atomistic processes at the interface to the mesoscale transport by a redistribution flux controlled by the so called "interface permeability" was developed. The model was validated with experimental data from diffusion couples. Calculations of the concentration profiles of the species at the electrode–electrolyte interface are reported. Active particle size, morphology and spatial arrangement were put in correlation with diffusion behavior for use in reverse engineering. DOI:10.1557/mrc.2016.31

RESEARCH LETTERS

Atom probe tomography of phosphorus- and boron-doped silicon nanocrystals with various compositions of silicon rich oxide

Keita Nomoto, University of New South Wales, Australia; **Sebastian Gutsch**, IMTEK, Albert-Ludwigs-Universität Freiburg, Germany; **Anna V. Ceguerr** and **Andrew Breen**, The University of Sydney, Australia; **Hiroshi Sugimoto** and **Minoru Fujii**, Kobe University, Japan; **Ivan Perez-Wurfl**, University of New South Wales, Australia; **Simon P. Ringer**, The University of Sydney, Australia; and **Gavin Conibeer**, University of New South Wales, Australia

We analyze phosphorus (P)- and boron (B)-doped silicon nanocrystals (Si NCs) with various compositions of silicon-rich oxide using atom probe tomography. By creating Si iso-concentration surfaces, it is confirmed that there are two types of Si NC networks depending on the amount of excess Si. A proximity histogram shows that P prefers to locate inside the Si NCs, whereas B is more likely to reside outside the Si NCs. We discuss the difference in a preferential location between P and B by a segregation coefficient. DOI:10.1557/mrc.2016.37

For more information or to submit your manuscript for review, visit:
www.mrs.org/mrc.

Dependence of confined plastic flow of polycrystalline Cu thin films on microstructure

Yang Mu and **Xiaoman Zhang**, Louisiana State University, USA; **J.W. Hutchinson**, Harvard University, USA; and **W.J. Meng**, Louisiana State University, USA

Axial compression was conducted on micro-pillars, in which polycrystalline Cu thin films were sandwiched between CrN and Si. Plastic flow of Cu was achieved, when the Cu films are inclined either at 90° or 45° with respect to the pillar axis. The texture of Cu films was altered by changing the template on which film growth occurred. The Cu microstructure was further altered by post-deposition annealing. The flow stress shows little dependence on the film texture in the as-deposited state. However, annealing influences the flow stress of confined Cu films significantly. The implications on strain gradient plasticity models are discussed. DOI:10.1557/mrc.2016.20

An augmented numerical inverse method for determining the composition-dependent interdiffusivities in alloy systems by using a single diffusion couple

Weimin Chen, **Jing Zhong**, and **Lijun Zhang**, Central South University, China

By solving the problems in the previous pragmatic method [*Scr. Mater*. 90–91, 53–56 (2014)] and including the interdiffusion flux as the criteria, an augmented numerical inverse method was proposed and realized in a house-made code. The proposed augmented numerical inverse method was successfully applied to high-throughput determination of the composition-dependent interdiffusivities in different solid solution alloys ranging from binary, ternary to multicomponent systems by using a single diffusion couple. Moreover, the advance features of the augmented numerical inverse method were also demonstrated. DOI:10.1557/mrc.2016.21

Combining *in situ* and online approaches to monitor interfacial processes in lubricated sliding contacts

Pantcho Stoyanov, Fraunhofer-Institute for Mechanics of Materials IWM—MicroTribology Center μTC and Karlsruhe Institute of Technology KIT, Germany; **J. Michael Shockley**, McGill University, Canada; **Martin Dienwiebel**, Fraunhofer-Institute for Mechanics of Materials IWM—MicroTribology Center μTC and Karlsruhe Institute of Technology KIT, Germany; and **Richard R. Chromik**, McGill University, Canada

In this study, "within the environment" and "within the contact" *in situ* tribology techniques are combined in order to study the interfacial processes in lubricated metallic (i.e., aluminum-based) sliding conditions. The evolution of the roughness follows the trend of the coefficient of friction closely, with initially low values followed by higher roughness during steady state. Similarly, the transfer film behavior correlates well with the roughness of the worn surfaces and the subsurface microstructure of the worn surfaces. The effect of normal load on the running-inbehavior is also studied in terms of differences in the interfacial processes. DOI:10.1557/mrc.2016.35

https://doi.org/10.1557/mrs.2016.212 Published online by Cambridge University Press